References and Notes

1. P. Zoller, J. I. Cirac, L. Duan, J. J. García-Ripoll, in *Les Houches 2003: Quantum Entanglement and Information Processing*, D. Estève, J.-M. Raimond, J. Dalibard, Eds. (Elsevier, Amsterdam, 2004), pp. 187–222.
2. M. Riebe *et al.*, *Nature* **429**, 734 (2004).
3. M. D. Barrett *et al.*, *Nature* **429**, 737 (2004).
4. J. Chiaverini *et al.*, *Nature* **432**, 602 (2004).
5. O. Mandel *et al.*, *Nature* **425**, 937 (2003).
6. E. Knill, R. Laflamme, G. J. Milburn, *Nature* **409**, 46 (2001).
7. J. P. Dowling, J. D. Franson, H. Lee, G. J. Milburn, *Quantum Inf. Process.* **3**, 205 (2004).
8. I. Protsenko, G. Reymond, N. Schlosser, P. Grangier, *Phys. Rev. A.* **66**, 062306 (2002).
9. C. Simon, W. T. M. Irvine, *Phys. Rev. Lett.* **91**, 110405 (2003).
10. L.-M. Duan, H. J. Kimble, *Phys. Rev. Lett.* **90**, 253601 (2003).
11. Y. L. Lim, A. Beige, L. C. Kwek, in press; preprint available at http://arXiv.org/abs/quant-ph/0408043.
12. B. B. Blinov, D. L. Moehring, L.-M. Duan, C. Monroe, *Nature* **428**, 153 (2004).
13. Single Photons on Demand, P. Grangier, B. Sanders, J. Vukovic, Eds. *New J. Phys.* **6**, 85–100, 129–163 (2004).
14. A. Kuhn, M. Hennrich, G. Rempe, *Phys. Rev. Lett.* **89**, 067901 (2002).
15. J. McKeever *et al.*, *Science* **303**, 1992 (2004).
16. M. Keller, B. Lange, K. Hayasaka, W. Lange, H. Walther, *Nature* **431**, 1075 (2004).
17. S. Bergamini *et al.*, *J. Opt. Soc. Am. B* **21**, 1889 (2004).
18. N. Schlosser, G. Reymond, I. Protsenko, P. Grangier, *Nature* **411**, 1024 (2001).
19. N. Schlosser, G. Reymond, P. Grangier, *Phys. Rev. Lett.* **89**, 023005 (2002).
20. We performed a full calculation of the second-order correlation function using the Heisenberg-Langevin equations, which gives the areas of the peaks. We also calculated the photon emission probabilities using density matrix and Monte Carlo methods, which lead to the same result.

21. We thank P. Georges for his assistance in designing the pulsed laser system. This work was supported by the European Union through the Information Society Technologies/Future and Emerging Technologies/Quantum Information Processing and Communications project "QGATES" and the Research Training Network "CONQUEST."

Supporting Online Material

www.sciencemag.org/cgi/content/full/309/5733/454/DC1
SOM Text

11 April 2005; accepted 25 May 2005
10.1126/science.1113394

Structural Relaxation of Polymer Glasses at Surfaces, Interfaces, and In Between

Rodney D. Priestley,[1] Christopher J. Ellison,[1] Linda J. Broadbelt,[1]* John M. Torkelson[1,2]*

We analyzed the glassy-state structural relaxation of polymers near surfaces and interfaces by monitoring fluorescence in multilayer films. Relative to that of bulk, the rate of structural relaxation of poly(methyl methacrylate) is reduced by a factor of 2 at a free surface and by a factor of 15 at a silica substrate interface; the latter exhibits a nearly complete arresting of relaxation. The distribution in relaxation rates extends more than 100 nanometers into the film interior, a distance greater than that over which surfaces and interfaces affect the glass transition temperature.

When cooled below the glass transition temperature (T_g), an amorphous material has higher specific volume, enthalpy, and entropy than in its equilibrium state at the same temperature. The resulting material is called a glass, which relaxes toward thermodynamic equilibrium in a process called structural relaxation (*1–3*). With polymers, glassy-state structural relaxation, often referred to as physical aging (*4–6*), can result in a time dependence of end-use properties of critical technological importance (*4–7*) such as increased modulus, increased brittleness, and reduced permeability. This glassy-state structural relaxation can be distinguished from the cooperative motion associated with T_g; the latter is associated with the α-relaxation [i.e., relaxation of cooperatively rearranging regions of some tens to hundreds of repeat units (*1*, *8*, *9*)], whereas the former has been commonly associated with the β-relaxation (*6*) (i.e., subsegmental relaxation such as the reorientation of an ester side group).

The glassy state and its associated phenomena, T_g and structural relaxation, are central challenges in condensed-matter physics (*10–14*) and are important in fields as varied as optical materials and the preservation of food and insect life (*11*, *12*). Numerous studies have established that confinement of amorphous materials between surfaces and interfaces at a length scale on the order of 100 nm can change T_g relative to its bulk value (*9*, *15–29*), whereas a limited number of studies have provided examples in which T_g is independent of confinement (*30*, *31*). Although many advanced technologies and materials (e.g., thin-film and asymmetric membranes and polymer nanocomposites) demand the long-time use of confined glasses (*4*, *28*, *29*), few studies have characterized the effect of nanoconfinement on structural relaxation in the glassy state.

Relative to bulk systems, enthalpy relaxation studies have indicated accelerated structural relaxation of a low molecular weight glass, *ortho*-terphenyl, confined to nanopores 11 to 12 nm in diameter (*32*). Physical aging in ultrathin polystyrene films was shown to be dependent on thickness and absent when the aging temperature was above the T_g of the confined film but below that of bulk polymer (*33*, *34*). In contrast, the presence of structural relaxation was observed above the bulk T_g for an ultrathin poly(methyl methacrylate) (PMMA) film supported on a silica substrate (*34*). The latter result was obtained because confinement leads to an increase in T_g due to attractive polymer-substrate interactions [hydrogen bond formation (*25*) between hydroxyl groups on the substrate surface and the polymer repeat unit]. Other investigations found little impact of confinement on structural relaxation of supported poly(isobutyl methacrylate) films (*18*) or superposed studies of structural relaxation with solvent evaporation in the case of supported PMMA films (*35*).

There is now substantial evidence that the origin of the T_g-nanoconfinement effect is related to surfaces and interfaces modifying relevant T_g dynamics in the interior regions of glass formers (*20*). Here, we report how surfaces and interfaces modify structural relaxation and to what extent these effects extend into the film interior. We use a fluorescence method in which dye-labeled polymer is inserted into known positions in a film in order to study the glassy-state relaxation dynamics. The dyes exhibit fluorescence intensities that increase substantially with minute increases in local density near the dye (*36*) and thereby provide an amplified sensitivity to structural relaxation. The method provides for highly sensitive, continuous monitoring of aging as well as the ability to measure aging rate distributions near surfaces, near interfaces, and in between. The distributions have been obtained with the use of 4-tricyanovinyl-[*N*-(2-hydroxyethyl)-*N*-ethyl]aniline (TC1)–labeled PMMA in single layers of multilayer PMMA films (*37*). We chose TC1 dye for the present study because its molecular structure allows for conformational mobility, which yields a high sensitivity of the dye fluorescence to the small densification that accompanies physical aging (*34*, *36*).

Figure 1 shows the increase in fluorescence intensity during relaxation at 305 K of a 400-nm-thick TC1-labeled PMMA film [T_g(bulk) = 393 K]. In agreement with specific volume and enthalpy relaxation measurements during physical aging of bulk polymer (*7*, *38*), the fluorescence intensity is roughly linear with logarithmic aging time. The intensity increases

[1]Department of Chemical and Biological Engineering, [2]Department of Materials Science and Engineering, Northwestern University, Evanston, IL 60208, USA.

*To whom correspondence should be addressed. E-mail: broadbelt@northwestern.edu; j-torkelson@northwestern.edu

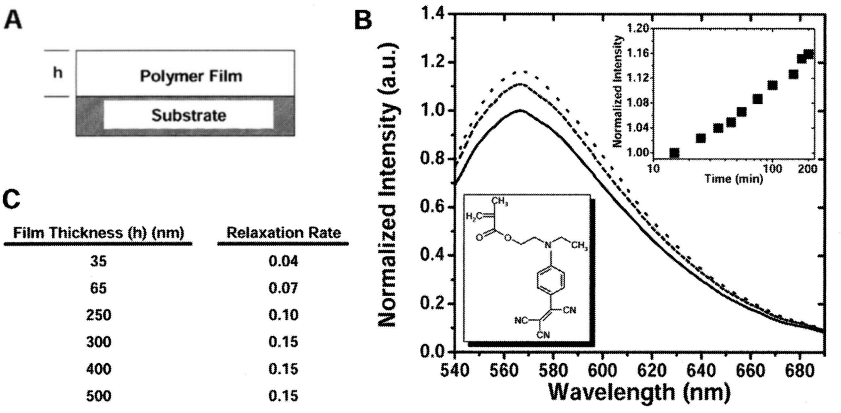

Fig. 1. Physical aging in single-layer PMMA films monitored via fluorescence. (**A**) Schematic of thin-film geometry. (**B**) Fluorescence emission spectrum of a 400-nm-thick TC1-labeled PMMA film after quenching from 418 K to 305 K taken after aging times of 15 min (solid curve), 100 min (dashed curve), and 200 min (dotted curve). Upper inset: Normalized fluorescence intensity at the maximum as a function of aging time. Lower inset: Molecular structure of TC1-labeled methacrylate monomer used in labeling PMMA. (**C**) Fluorescence aging/structural relaxation rate defined by Eq. 1 as a function of film thickness (h) for TC1-labeled PMMA at 305 K. Data are averages of two runs with SD of 0.01 or less.

16% (after a quench from 418 K to 305 K) as aging time increases from 15 min to 200 min. By analogy with physical aging rates based on volume relaxation (*7*, *38*), an aging rate based on fluorescence intensity, R_f, may be defined as

$$R_f = (1/F_o)[dF/d(\log t_a)] \quad (1)$$

where F is fluorescence intensity at aging time t_a, and F_o is intensity at reference time t_o. Aging rates are a nonlinear function of temperature and typically exhibit a maximum. The maximum aging rate is a result of the competition between thermodynamic driving forces for aging, which is highest at temperatures well below T_g, and subsegmental mobility, which increases with temperature (*38*).

The results in Fig. 1C were obtained by fitting data similar to the upper inset of Fig. 1B to Eq. 1 for TC1-labeled single-layer PMMA films. The aging rate at 305 K increases by a factor of ~4 upon increasing film thickness from 35 nm to 300 nm (Fig. 1C). For film thicknesses ≥ 300 nm, R_f is independent of thickness and is equal to the relaxation rate of 0.15 obtained for a TC1-labeled PMMA film several μm thick, representative of bulk. [All values of the relaxation rate R_f, which is unitless, are determined via Eq. 1 with aging time t_a in units of minutes.] Although the sensitivity of TC1 fluorescence to aging is tied to volume relaxation [minute increases in local density near TC1 reduce the rate of nonradiative decay from the TC1 excited state, resulting in enhanced fluorescence (*34*, *36*)], the physical aging rate determined via TC1 fluorescence is amplified by orders of magnitude relative to that determined from volume relaxation. For example, the specific volume relaxation rate, R_v, of bulk PMMA is ~0.00055 during aging at 305 K (*38*). The specific volume relaxation rate is defined (*38*) as

$$R_v = -(1/V_o)[dV/d(\log t_a)] \quad (2)$$

where V is specific volume at t_a, and V_o is specific volume at t_o. Over an aging time from 20 min to 200 min, this means that bulk PMMA at 305 K undergoes a 0.055% reduction in specific volume. Relative to R_v, R_f is greater by a factor of ~275 during physical aging at the same conditions.

We used multilayer films to explore the influence of confining substrate and free surfaces on glassy-state relaxation. Figure 2 shows structural relaxation data from a 25-nm-thick TC1-labeled PMMA middle layer sandwiched between two 1000-nm-thick PMMA layers (Fig. 2A), from a 25-nm-thick TC1-labeled free-surface layer sitting atop a 1000-nm-thick PMMA underlayer (Fig. 2B), and from a 25-nm-thick TC1-labeled substrate layer sandwiched between a 1000-nm-thick PMMA overlayer and the substrate (Fig. 2C). At 305 K, the relaxation rate is greatest in the middle layer, yielding $R_f = 0.14$, equal within error to that in bulk, and is reduced by a factor of 2 at the free surface. The substrate layer exhibits the slowest relaxation rate of 0.01 at 305 K, indicating that physical aging is almost totally suppressed next to the substrate.

At an aging temperature of 388 K, the free-surface layer exhibits almost no relaxation. This near-absence of aging is consistent with the notion that much of the 25-nm-thick free-surface layer has a T_g that is equal to or below 388 K and suggests that there is a rubbery equilibrium layer at the free surface. As the aging temperature is decreased, structural relaxation becomes more pronounced at the free surface but is always substantially less than that in the interior of the film. In

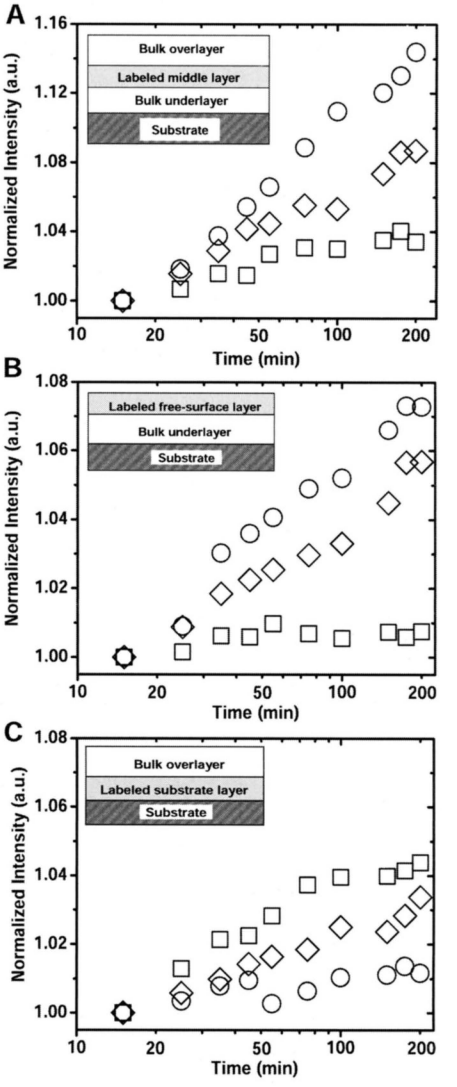

Fig. 2. Physical aging monitored by fluorescence in multilayer PMMA films with 25-nm-thick TC1-labeled layers and 1000-nm-thick unlabeled bulk overlayers/underlayers. Insets show schematics of the film arrangement. Normalized fluorescence intensity is shown as a function of aging time for a trilayer film (**A**) and two bilayer films (**B** and **C**) aged at 305 K (circles), 348 K (diamonds), and 388 K (squares). Data points are averages of two runs.

contrast, the substrate layer exhibits an increasing relaxation rate with increasing temperature and at 388 K has nearly the same rate as the middle layer. The additional thermal energy at higher temperatures approaching T_g likely reduces the ability of interfacial hydrogen bonds to suppress aging.

Further understanding of the impact of confinement on physical aging is obtained via buried-layer experiments, where 25-nm-thick TC1-labeled middle layers are placed a distance from the free surface or substrate interface. Figure 3 shows results from trilayer studies at 305 K. As a 25-nm-thick layer is moved from the free surface to a buried layer, there is a smooth increase in relaxation rate,

from 0.07 at the free surface to 0.08, 0.11, and 0.15 when buried 25 nm, 100 nm, and 250 nm, respectively, below the free surface (Fig. 3A). Within error (±0.01), the relaxation rate in the layer buried 250 nm below the free surface is identical to bulk. The rate of structural relaxation increases sharply from 0.01, when a 25-nm-thick layer is located next to the substrate, to 0.10, when located 25 nm from the substrate (Fig. 3B). Further displacement results in a smooth increase in relaxation rate, from 0.12 to 0.14 when the layer is located 100 nm and 250 nm, respectively, from the substrate. Thus, the substrate and free surface affect the structural relaxation rate in supported PMMA films over similar distances, but the substrate interactions perturb the structural relaxation to a greater extent.

Our results are consistent with a schematic (Fig. 4) of the surface- and interface-induced gradients in relaxation. At a distance of at least 100 nm but less than 250 nm from the free surface, there begins a smooth factor-of-2 reduction in structural relaxation rate between the bulk and the free surface. At a distance of at least 100 nm but less than 250 nm from the substrate interface, there begins a factor-of-15 reduction in relaxation rate from the bulk to the interface, the vast majority of which occurs within 25 nm of the interface. The origins of the perturbations near the free surface and substrate differ. Near the free surface, there is enhanced cooperative segmental mobility and a reduced T_g (*20*), resulting in a reduced thermodynamic driving force for structural relaxation. At the substrate interface, hydrogen bonds suppress cooperative segmental mobility and lead to an increased T_g (*25*). Hence, there is an enhanced thermodynamic driving force for structural relaxation. However, the interfacial hydrogen bonds also suppress smaller motions associated with structural relaxation; deep in the glassy state, this suppression can result in near-elimination of physical aging within 25 nm of the substrate and retardation of aging relative to bulk at a distance of at least 100 nm from the substrate. The manner in which retardation in aging occurs over distances of at least 100 nm from a substrate or free surface is not yet understood, but it may relate to the percolation of slowly relaxing dynamic heterogeneities that has been hypothesized as an explanation for the effect of confinement on T_g (*21*, *22*, *39*) and that is expected to result in long-range changes in dynamics induced by surfaces and interfaces (*39*). No current theory or model directly addresses the effect of confinement on glassy-state structural relaxation.

It is important to note that the distribution of glassy-state structural relaxation rates that we obtained is distinct from the distribution of T_g values in supported PMMA films. Although a determination of the full distribution of T_g values is beyond the scope of this study, selected measurements of T_g values have been obtained in experiments that equate T_g to the intersection of the rubbery- and glassy-state temperature dependences of fluorescence intensity (*20*). Relative to bulk T_g (393 K), a 25-nm-thick layer at the free surface of a 1000-nm-thick film exhibits a reduction in T_g of 5 to 6 K, whereas a 25-nm-thick layer at the substrate of a 1000-nm-thick film exhibits an increase in T_g of 12 K. However, the T_g of a 25-nm-thick layer that is located 100 nm from either the substrate interface or the free surface in an 800-nm-thick multilayer film is identical within error (±1 K per sample) to the T_g of bulk TC1-labeled PMMA. Thus, interfacial effects perturb glassy-state structural relaxation rates 100 nm from the substrate, but they do not perturb T_g values over the same length scale. This is possibly because T_g is associated with larger scale motions of cooperative segmental mobility (α-relaxation processes), whereas glassy-state structural relaxation may be associated with different, smaller-scale dynamics (β-relaxation processes) (*6*). Novel experiments need to be developed to characterize directly how α- and β-relaxation dynamics near T_g are separately affected by surfaces and interfaces. Our results suggest that surface and interface effects may potentially be tailored to control the structural relaxation of high-performance materials that have a large fraction of polymer near surfaces and interfaces, as with polymer nanocomposites.

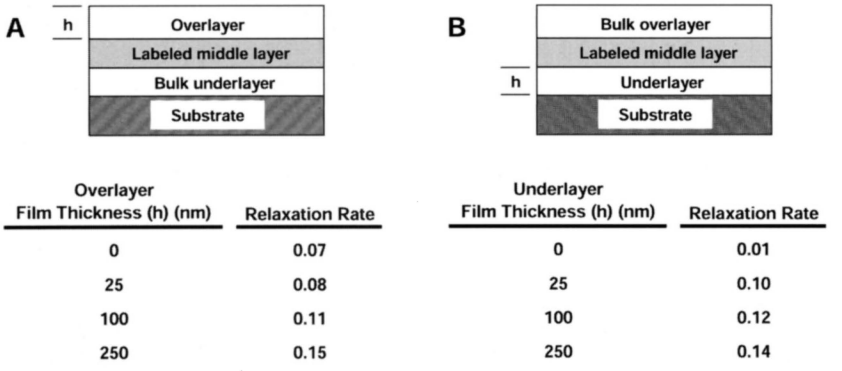

Overlayer Film Thickness (h) (nm)	Relaxation Rate
0	0.07
25	0.08
100	0.11
250	0.15

Underlayer Film Thickness (h) (nm)	Relaxation Rate
0	0.01
25	0.10
100	0.12
250	0.14

Fig. 3. Structural relaxation rates at 305 K for PMMA multilayer films with a 25-nm-thick TC1-labeled layer. The trilayer films characterize relaxation rates at known distances from free surfaces and substrate interfaces. Bulk overlayers and underlayers are 700 nm thick for trilayer films and 1000 nm thick for bilayer films. (**A** and **B**) Fluorescence relaxation rates of a TC1-labeled layer placed (A) at the free surface or at distances below the free surface (25, 100, and 250 nm) and (B) at the substrate or at distances from the substrate (25, 100, and 250 nm). Data are averages of two runs with SD of 0.01 or less.

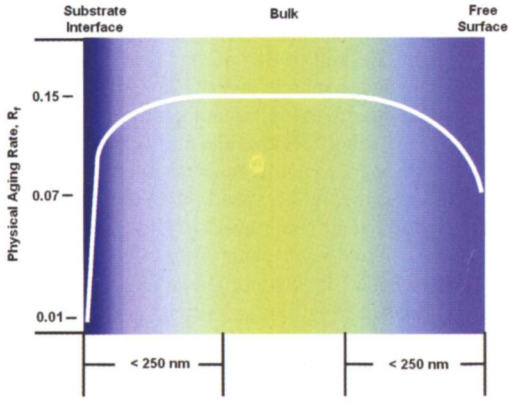

Fig. 4. Representation of the effect of the substrate interface and the free surface on the distribution of structural relaxation rates in PMMA at 305 K. Both the substrate interface and the free surface perturb the relaxation rate at least 100 nm but less than 250 nm into the film interior. Relative to bulk behavior, a 25-nm-thick layer at the free surface exhibits a factor-of-2 reduction in relaxation rate. In contrast, a 25-nm-thick layer at the substrate interface exhibits a factor-of-15 reduction in relaxation rate relative to bulk (i.e., almost a complete arresting of physical aging). Color gradations indicate continuous nature of change in aging rate (bright green, high rate; dark blue, low rate) in bulk.

References and Notes

1. C. A. Angell, K. L. Ngai, G. B. McKenna, P. F. McMillan, S. W. Martin, *J. Appl. Phys.* **88**, 3113 (2000).
2. E. R. Weeks, J. C. Crocker, A. C. Levitt, A. Schofield, D. A. Weitz, *Science* **287**, 627 (2000).
3. R. Torre, P. Bartolini, R. Righini, *Nature* **428**, 296 (2004).
4. Y. Huang, D. R. Paul, *Polymer* **45**, 8377 (2004).
5. J. Kurchan, *Nature* **433**, 222 (2005).
6. L. C. E. Struik, *Physical Aging in Amorphous Polymers and Other Materials* (Elsevier, New York, 1978).
7. J. M. Hutchinson, *Prog. Polym. Sci.* **20**, 703 (1995).
8. G. Adam, J. H. Gibbs, *J. Chem. Phys.* **43**, 139 (1965).
9. C. J. Ellison, M. K. Mundra, J. M. Torkelson, *Macromolecules* **38**, 1767 (2005).
10. J. I. Brauman, *Science* **267**, 1887 (1995).
11. P. G. Debenedetti, F. H. Stillinger, *Nature* **410**, 259 (2001).
12. C. A. Angell, *Science* **267**, 1924 (1995).
13. V. N. Novikov, A. P. Sokolov, *Nature* **431**, 961 (2004).
14. P. G. de Gennes, *Eur. Phys. J. E* **2**, 201 (2000).
15. C. L. Jackson, G. B. McKenna, *J. Non-Cryst. Solids* **131-133**, 221 (1991).
16. J. L. Keddie, R. A. L. Jones, R. A. Cory, *Europhys. Lett.* **27**, 59 (1994).
17. J. A. Forrest, K. Dalnoki-Veress, J. R. Stevens, J. R. Dutcher, *Phys. Rev. Lett.* **77**, 2002 (1996).
18. C. J. Ellison, S. D. Kim, D. B. Hall, J. M. Torkelson, *Eur. Phys. J. E* **8**, 155 (2002).
19. B. Jerome, J. Commandeur, *Nature* **386**, 589 (1997).

20. C. J. Ellison, J. M. Torkelson, *Nat. Mater.* **2**, 695 (2003).
21. S. Merabia, P. Sotta, D. Long, *Eur. Phys. J. E* **15**, 189 (2004).
22. A. R. C. Baljon, J. Billen, R. Khare, *Phys. Rev. Lett.* **93**, 255701 (2004).
23. F. Varnik, J. Baschnagel, K. Binder, *Phys. Rev. E* **65**, 021507 (2002).
24. T. S. Jain, J. J. de Pablo, *Phys. Rev. Lett.* **92**, 155505 (2004).
25. C. W. Frank *et al.*, *Science* **273**, 912 (1996).
26. C. B. Roth, J. R. Dutcher, in *Soft Materials: Structure and Dynamics*, J. R. Dutcher, A. G. Marangoni, Eds. (Dekker, New York, 2005).
27. M. Alcoutlabi, G. B. McKenna, *J. Phys. Condens. Matter* **17**, R467 (2005).
28. B. J. Ash, L. S. Schadler, R. W. Siegel, *Mater. Lett.* **55**, 83 (2002).
29. J. Berriot *et al.*, *Macromolecules* **35**, 9756 (2002).
30. P. A. O'Connell, G. B. McKenna, *Science* **307**, 1760 (2005).
31. C. J. Ellison, R. L. Ruszkowski, N. J. Fredin, J. M. Torkelson, *Phys. Rev. Lett.* **92**, 095702 (2004).
32. S. L. Simon, J. Y. Park, G. B. McKenna, *Eur. Phys. J. E* **8**, 209 (2002).
33. S. Kawana, R. A. L. Jones, *Eur. Phys. J. E* **10**, 223 (2003).
34. R. D. Priestley, L. J. Broadbelt, J. M. Torkelson, *Macromolecules* **38**, 654 (2005).
35. H. Richardson, I. Lopez-Garcia, M. Sferrazza, J. L. Keddie, *Phys. Rev. E* **70**, 051805 (2004).
36. J. S. Royal, J. M. Torkelson, *Macromolecules* **26**, 5331 (1993).
37. See supporting data on *Science* Online.
38. R. Greiner, F. R. Schwarzl, *Rheol. Acta* **23**, 378 (1984).
39. D. Long, F. Lequeux, *Eur. Phys. J. E* **4**, 371 (2001).
40. Supported by the NSF Materials Research Science and Engineering Center program at Northwestern University (grant DMR-0076097), a GEM Fellowship (R.D.P.), and a Henderson Dissertation Year Fellowship (C.J.E.).

Supporting Online Material
www.sciencemag.org/cgi/content/full/309/5733/456/DC1
Materials and Methods
References

14 March 2005; accepted 24 May 2005
10.1126/science.1112217

Simulations of a Quasi–Taylor State Geomagnetic Field Including Polarity Reversals on the Earth Simulator

Futoshi Takahashi,[1]* Masaki Matsushima,[2] Yoshimori Honkura[2]

High-resolution, low-viscosity geodynamo simulations have been carried out on the Earth Simulator, one of the fastest supercomputers, in a dynamic regime similar to that of Earth's core, that is, in a quasi–Taylor state. Our dynamo models exhibit features of the geodynamo not only in spatial and temporal characteristics but also in dynamics. Polarity reversals occurred when magnetic flux patches at high latitudes moved poleward and disappeared; patches with reversed field at low and mid-latitudes then moved poleward.

A dynamo process in Earth's fluid outer core, known as the geodynamo, is believed to generate Earth's intrinsic magnetic field. Numerical simulations of the geodynamo have been performed (*1*–*5*), and dynamo models have shown some similarity to the geomagnetic field (*6*, *7*), including polarity reversals (*1*, *2*, *5*, *8*). It is still unclear whether these models accurately reproduce the dynamics of Earth's outer core, because the simulations were performed at a dynamic regime much different from that of the core. The most essential parameter of the dynamic regime is the Ekman number, E, which represents the relative importance of viscosity to the rotation rate; its value is extremely small ($E \sim 10^{-9}$) for Earth's core. Previously, artificial treatments were needed to perform effective computations (*9*).

Taylor (*10*) showed that the magnetic field in the core varies such that the axial magnetic torque on cylindrical surfaces that are coaxial with the rotation axis is small, because it can be balanced only with the extremely small viscous and inertial torques. The limit of vanishing viscosity leads to the so-called Taylor's constraint that the axial magnetic torque must vanish. The dynamo satisfying Taylor's constraint is considered to be in a Taylor state. In reality, the geodynamo is in a quasi–Taylor state, in which the effect of viscosity plays a negligibly small role in core dynamics (*11*).

To obtain such a quasi–Taylor state dynamo, one must carry out high-resolution numerical simulations for lower viscosity, which are prohibitively time-consuming even on most supercomputers. The Earth Simulator alleviates this situation and is capable of reaching an Ekman number of 4×10^{-7}; our results are mostly based on computations for a slightly higher value, $E = 4 \times 10^{-6}$, in the definition of Kono and Roberts (*12*) using the core radius as a length scale. We used the spectral method to solve magnetohydrodynamic equations (*13*–*15*). The spatial resolution is ensured by including all the constituents of spherical harmonics up to degree and order 255.

We performed simulations for various values of the Rayleigh number Ra (*13*) and evaluated the resulting dynamo models with

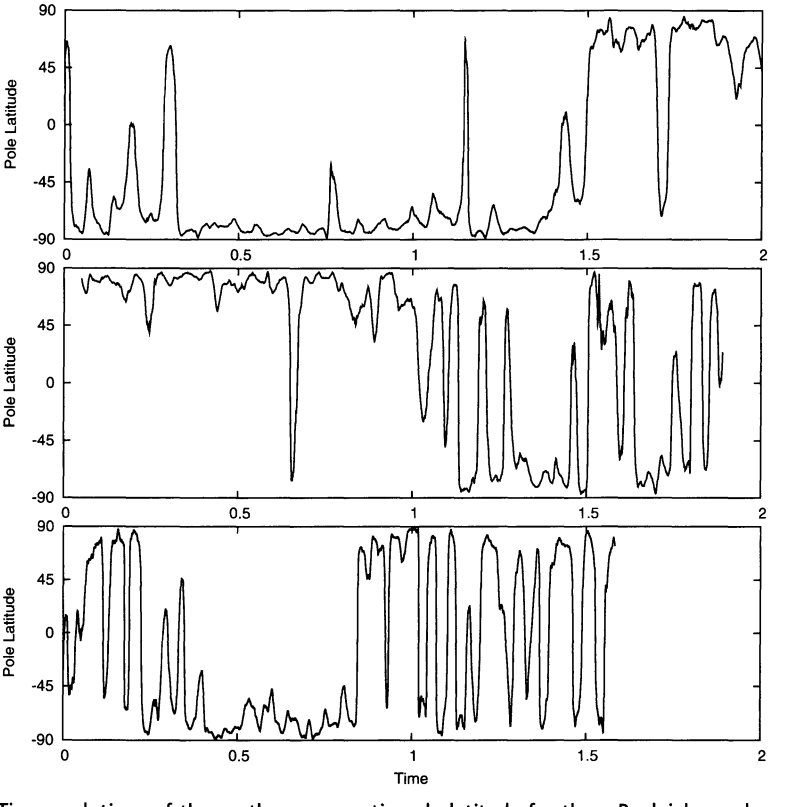

Fig. 1. Time evolutions of the north geomagnetic pole latitude for three Rayleigh numbers, $Ra = 1.57 \times 10^8$ (top), $Ra = 1.96 \times 10^8$ (middle), and $Ra = 2.35 \times 10^8$ (bottom). Time is scaled by the magnetic diffusion time t_m, corresponding to roughly 200,000 years.

[1]Institute of Space and Astronautical Science, Japan Aerospace Exploration Agency, 3-1-1 Yoshinodai, Sagamihara, Kanagawa, Japan. [2]Department of Earth and Planetary Sciences, Tokyo Institute of Technology, 2-12-1 Ookayama, Meguro-ku, Tokyo, Japan.

*To whom correspondence should be addressed. E-mail: futoshi@stp.isas.jaxa.jp